# Lanthanide Isophthalate Metal-Organic Frameworks: Crystal Structure, Thermal Behavior, and White Luminescence

Virgile Trannoy, Isis N'Dala-Louika, Jérôme Lhoste, Thomas Devic, Hélène Serier-Brault

# Lanthanide isophthalate metal-organic frameworks: crystal structure, thermal behavior and white luminescence properties

*Virgile Trannoy*[*†], *Isis N'Dala-Louika*[†], *Jérôme Lhoste*[±], *Thomas Devic*[†], *Hélène Serier-Brault*[*,†]

† Dr. V. Trannoy, Ms. I. N'Dala-Louika, Dr. T. Devic, Dr. H. Serier-Brault

Université de Nantes, CNRS, Institut des Matériaux Jean Rouxel, IMN, F-44000 Nantes, France.

± Dr. J. Lhoste

Université du Maine, Institut des Molécules et Matériaux du Mans, UMR CNRS 6283, Avenue Olivier Messiaen, 72085 Le Mans, France.

**Corresponding Author**

helene.brault@cnrs-imn.fr https://www.cnrs-imn.fr/index.php/accueil-l-imn/annuaire-imn-membres-de-l-imn-par-noms-et-par-services/item/brault-helene

Twitter : @brault_helene

virgile.trannoy@lspm.cnrs.fr https://www.researchgate.net/profile/Virgile_Trannoy

Twitter : @VTrannoy

**Supporting Information**.

PXRD, FT-IR, TGA, thermodiffraction analyses, lattice parameters evolution with the temperature, PL spectra and CIE diagram and some crystal parameters (PDF).

**ABSTRACT** Two novel lanthanide metal-organic frameworks (LnMOFs), $Ln_{1.14}Na_{0.57}(BDC)_2(H_2O)\cdot 4H_2O$ (Ln = $La^{3+}$ or $Ce^{3+}$, BDC : 1,3-benzenedicarboxylate), have been synthesized under hydrothermal conditions by using a $Ln^{3+}$ coordination polymer as precursor. The crystal structure was determined from single crystal X-ray diffraction. Both compounds are isostructural and contain chains of face-sharing [$LnO_{10}$] polyhedra connected by the linkers to form an anionic three-dimensional network, defining both polar and apolar channels, the latter being occupied by water molecules and $Ln^{3+}$ and $Na^{+}$ cations. When doped by optimized content of $Eu^{3+}$ and $Tb^{3+}$, the $La^{3+}$ counterpart exhibits white luminescence emission with CIE parameters equal to (0.3440, 0.3735) at $\lambda_{exc}$ = 321 nm, which renders the material attractive for white LED application.

## INTRODUCTION

Lanthanide-based MOFs (LnMOFs) are considered as promising functional materials for optical properties, especially due their luminescent properties that can be used for applications such as chemical or temperature sensing, lightings, displays[1–8]… Recently, LnMOFs have attracted increasing attention in the active field of single-phase white light emission materials[9–18]. Compared to the inorganic phosphors, LnMOFs compounds offer many advantages for the elaboration of new single-phase phosphors such as their slow temperature synthesis, the efficient antenna effect of the ligand, and the ease to homogenously co-dope by $Ln^{3+}$ cation to generate

various emission colors[19]. To conceive a single-phase white-luminescent MOF material, a promising approach consists in tuning the proportion of the blue emission of the organic ligand, the green light from $Tb^{3+}$ cation and the red color from $Eu^{3+}$ cation[11,13–18,20–26]. The tuning of relative proportion of each color can be optimized by adjusting the different amounts of the red and green emitters, but also by an adjustment of the excitation wavelength in order to modulate the blue emission of the ligand and obtain the required white emission[12,20].

For an efficient energy transfer from an organic linker to $Eu^{3+}$ and $Tb^{3+}$ ions, the ligand should have suitable triplet excited-state energy (between 22000 and 27000 $cm^{-1}$) matching the energy of the main accepting levels of $Eu^{3+}$ ($^5D_1$: 19030 $cm^{-1}$) and $Tb^{3+}$ ($^5D_4$: 20500 $cm^{-1}$)[3]. In this purpose, aromatic carboxylate acids are usually chosen as photosensitizers to construct the LnMOFs compounds. Targeting an application such as white LED lightening, efforts must be done to develop efficient materials with a relative low synthesis cost. In this context, we focus our attention on an inexpensive commercially available organic ligand, namely 1,3-benzenedicarboxylic acid, or isophthalic acid. This common linker is a rigid carboxylate ligand which enables various coordination modes to build MOF network [27–31], and which gets an appropriate triplet excited-state energy (27900 $cm^{-1}$).[32] Herein, we report the synthesis of two new isomorphous 3D lanthanide-bearing metal-organic frameworks built up from isophthalate (1,3-BDC), with the chemical composition $Ln_{1.14}Na_{0.57}(BDC)_2(H_2O)\cdot 4H_2O$ (Ln = $La^{3+}$ or $Ce^{3+}$). The crystal structure of both compounds was determined by single-crystal X-ray diffraction, while their thermal behavior was investigated by multiple techniques (TGA, IR spectroscopy, temperature-dependent XRD). Additionally, we successfully obtained a luminescent material with white light emission by codoping the $La^{3+}$ counterpart with $Tb^{3+}$ and $Eu^{3+}$ ions in appropriate proportions.

RESULTS AND DISCUSSION

## 1. Synthesis of the LnMOF

During the synthesis and before the hydrothermal treatment, the addition under stirring of the $Ln^{3+}$ salt into the limpid basic solution of the ligand leads to the formation of a white precipitate at pH = 5 and at room-temperature. The as-synthesized white powder obtained for $La^{3+}$ and $Ce^{3+}$ (**La-CP** and **Ce-CP**) were analyzed by PXRD, FTIR analysis and thermal analysis (Figures S1-S3). Firstly, the X-ray diffraction patterns (Figure S1) is identical to that of a cerium benzene-1,3-dicarboxylate compound reported by Zheng *et al.* [33] , and which was obtained by the reaction of of a $Ce(NO_3)_3$ aqueous solution with a solution a 4:1 ethanol-water solution of $H_2BDC$ at a pH = 7 (the pH being adjusted by the addition of ammonia solution). However, the crystal structure is unknown so far and a thorough search in the crystal structure database did not result in a convincing match. Nevertheless, efforts have been done to characterize this phase. Then, the FTIR spectroscopy (Figure S2) confirms the presence of solely deprotonated carboxylate groups (no band at ca. 1700 $cm^{-1}$, characteristic of free carboxylic groups), while the TGA analysis (Figure S3) shows at 100°C a first mass loss of 22.7%, and 23.5% for **La-CP** and **Ce-CP**, respectively, which can be attributed to the loss of water molecules. Moreover, complementary EDX measurements revealed the presence of sodium in the compounds with a cationic molar ratio Ln/Na (Ln = Ce or La) equal to 5, the sodium coming from the sodium hydroxide solution used to deprotonate the carboxylic acid. Additional elemental analyses confirmed a content of 29.35%, 3.721%, for C and H, respectively, in **La-CP**, and a content of 29.35%, 3.61%, for C and H, respectively, in **Ce-CP**, enabling to propose the molecular formula $Ln_{0.938}Na_{0.187}(C_8H_4O_4)_{1.5}\cdot 6H_2O$.

Under hydrothermal conditions (see experimental part), both coordination polymers, namely **La-CP** and **Ce-CP**, are transformed to small colorless single-crystals suitable for single crystal XRD analysis. **LaMOF** and **CeMOF,** which are isostructural. Hence, only the structure of the La counterpart is described in detail. The compound crystallizes in the tetragonal apolar space group $P4_22_12$. In the network, each La(1) cation is coordinated by ten oxygen atoms, eight oxygen atoms arising from the two different carboxylate groups and two oxygen atoms from water molecules in a distorted bicapped square prismatic environment (Figure 1a). The La(1)•••O bond distances range from 2.473(5) to 2.686(4) (2.452(6) to 2.710(11) pour **CeMOF**) Å for a bond valence equal to 3.18 for $La^{3+}$ cation (and 3.15 for $Ce^{3+}$ cation) (Table S3). In the structure, only one coordination mode exists, namely monodentate/tridentate-chelating-bridging (Figure S5), as confirmed by the FTIR spectroscopic analysis: while the C=O vibration band at 1693 $cm^{-1}$ characteristic free carboxylic group in $H_2BDC$ vanished, a shoulder at ca. 1680 $cm^{-1}$ associated with the dangling C=O bond is detected (Figure S4)[34].The coordination $La(1)O_{10}$ polyhedra are connected by a triangular face along the *c* axis to form infinite chains. Subsequently, each chain is linked to four others chains by the $BDC^{2-}$ ligand with a distance between metal centers equal to 11.231(1) along the *a* axis Å (11.197(2) pour **CeMOF**) (Figure 1b) to form a 3D MOF network with channels running along the *c* axis. The network exhibits alternating apolar and polar channels, the latter being occupied by disordered $Ln^{3+}$ and $Na^+$ cations surrounded by water molecules to provide a final chemical composition of $La_{1.14}Na_{0.57}(BDC)_2(H_2O)\cdot 4H_2O$. The presence of $Na^+$ cations was not expected and can be justified by the use of NaOH solution to dissolve and deprotonate the carboxylic acid during the synthetic process. The chemical composition was confirmed by elemental and thermal analyses, with a La/Na molar ratio increased to 2 after the hydrothermal process, while the number of water molecules represent 15.9% and 15.1% for **LaMOF** and

**CeMOF**, respectively (Figure S6). The comparison of the experimental powder XRD pattern of both MOFs with that calculated from the determined structure (Figure S7) confirms that both compounds were prepared as pure phases. Furthermore, distances between the non-coordinated oxygen atom from the carboxylate ligand and the coordinated water molecule $O_{w1}$ is equal to 2.699(9) Å (and 2.692(8) Å for **CeMOF**), indicating the presence of an hydrogen bond[35] (Figure 1c).

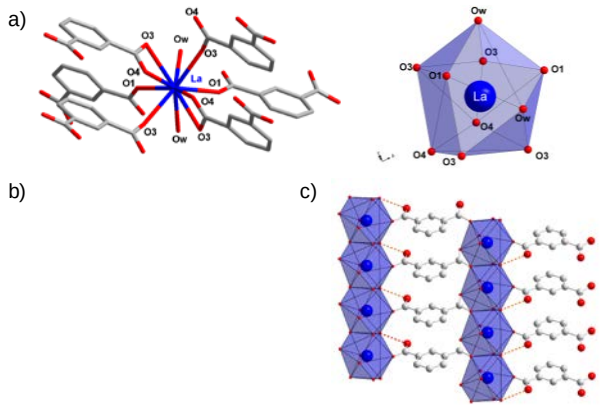


**Figure 1.** a) The coordination sphere of La in **LaMOF** forming a distorted bicapped square prism, b) Projection along the *c* axis of the **LaMOF** structure (blue: $LaO_{10}$ polyhedra, red: oxygen, yellow: sodium, grey: carbon, H atoms being omitted for clarity), c) H-bond (dotted red line) between the non-coordinated oxygen atom of the organic linker and the oxygen atom of the coordinated water molecule ($O_{W1}$).

**Table 1.** Summary of crystallographic data for the structures

| **Compounds** | $Ce_{1.14}Na_{0.57}C_{16}O_{13}H_{18}$ | $La_{1.14}Na_{0.57}C_{16}O_{13}H_{18}$ |
|---|---|---|
| Notation | **CeMOF** | **LaMOF** |
| Molecular weight (g $mol^{-1}$) | 591.1 | 588.7 |
| Crystal system | Tetragonal | |
| Space group | $P4_22_12$ | |
| a (Å) | 21.9543(13) | 22.0138(14) |
| c (Å) | 4.1070(3) | 4.1253(4) |
| V ($Å^3$), | 1979.5(3) | 1999.2(3) |
| Z, $\rho_{calc.}$ (g $cm^{-3}$) | 4, 1.984 | 4, 1.954 |
| Wavelength (Å) | $MoK_\alpha$ | $MoK_\alpha$ |
| $\mu$/mm-1 | 2.694 | 2.508 |
| 2θ range (°) | 4.0 – 56.4 | 4.1 – 60.0 |
| Limiting indices | $-27 \leq h \leq 28$<br>$-28 \leq k \leq 19$<br>$-5 \leq l \leq 5$ | $-29 \leq h \leq 23$<br>$-29 \leq k \leq 18$<br>$-5 \leq l \leq 5$ |
| Collected reflections | 17190 | 11290 |
| Refl. uni. | 2274 | 2898 |
| Refined parameters | 156 | 154 |
| Goodness-of-fit on $F^2$ | 1.014 | 1.104 |
| Final R indices [I>2σ(I)] | $R_1 = 0.0431$<br>$Rw_1 = 0.0845$ | $R_1 = 0.0505$<br>$Rw_1 = 0.0952$ |
| R indices (all data) | $R_1 = 0.0698$<br>$Rw_1 = 0.0953$ | $R_1 = 0.0921$<br>$Rw_1 = 0.1095$ |
| Largest diff. peak and hole/e.$Å^{-3}$ | 0.602/-0.753 | 0.755/-0.854 |

## 2. Thermal behavior of the LnMOF

The thermal behavior of both **LaMOF** and **CeMOF** was investigated by a multiple set of techniques. Fist, both TG curves exhibits a flat plateau above 150°C, whose position matches with the full dehydration of the solids (**CeMOF**: experimental and theoretical weight losses are 15.6% and 15.2% respectively; **LaMOF**: experimental and theoretical weight losses are 15.7% and 15.3% respectively) (Figure S8). X-ray powder thermodiffraction experiments were performed under ambient air from 30 to 200°C to investigate the dehydrated form. It showed that the water departure is associated with a major structural change at ca. 90°C and a significant decrease of crystallinity.

Pattern matching refinements (Le Bail method) were carried out for each temperature to follow the lattice parameters evolution. Surprisingly, all diffraction data could have been easily fitted by using the same lattice parameters of **LaMOF** and **CeMOF**, indicating that the crystal system and space group are maintained even for the dehydrated form. During the thermal treatment, the lattice volume decreases of 18.8% (Figure 2b) while the *a* and *c* parameters decrease of 7.3 and 5.6%, respectively (Figure S9). In the same way, the **CeMOF** compound exhibits a 21.2% decrease in volume (Figure S10) associated to a 7.1% and 8.7% decrease in *a* and *c* parameters (Figure S11), respectively. Unfortunately, the moderate crystallinity of the dehydrated forms precluded any structure refinement by Rietveld techniques. Nevertheless, nitrogen sorption experiments carried out a 77 K on the dehydrated solids resulted in a very low BET surface values ($\approx 9\ m^2/g$), indicative of non-porous solids. This suggests that the dehydration is accompanied with a shrinkage of the pores resulting from the reorganization of the coordination sphere around the cation, as commonly found in Ln-MOFs[36]. Considering the crystal structure, one can hypothesize that, upon departure of bound water molecule, the pendant carboxylate oxygen atom starts to interact with the Ln ions. This is in line with the FTIR analysis, which shows the disappearance of the shoulder at 1670 $cm^{-1}$ characteristic of the dangling C=O bond upon dehydration (Figure S12). It is also expected that, upon the loss of their hydration sphere, the cation embedded in the cavities, specially $Ln^{3+}$, will also strongly interact with the oxygen atom of the ligands, precluding the reopening of the channels. This dehydration process is indeed irreversible under air and the native LnMOF is not recovered in these conditions (Figure 2b). Finally, the irreversibility of the desolvation process was also probed immersing the dehydrated compound of **LaMOF** in various solvents for 2 hours, namely water, MeOH, $CH_3CN$ and DMF, and further analyzing its structure by PXRD in a capillary tube (Figure S13). For the three organic solvents, the structure is not modified, the volume

lattice (determined by Le Bail refinement) remains similar to the dehydrated form. Surprisingly, the immersion in water leads to a decomposition of the MOF and the formation of the initial coordination polymer **La-CP** as indicated by XRD and FTIR analyses (Figures S13 and S14).

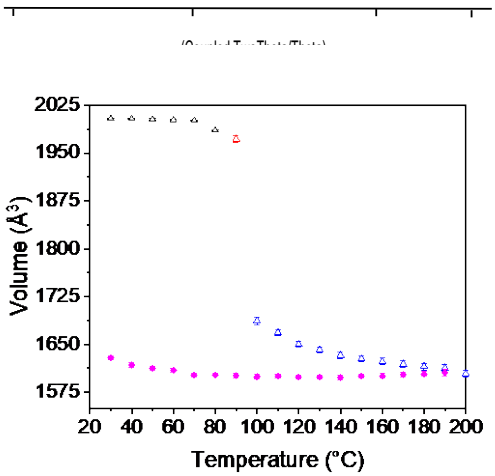


**Figure 2**. a) X-ray thermodiffractogram of **LaMOF** performed under air from 30°C to 200°C using a 10°C step. Black: as-synthesized form, blue: dehydrated form, red: mixture of the as-synthesized form and the dehydrated one. b) Lattice volume evolution with the temperature from 30 to 200°C (black, red and blue points) and from 200 to 30°C (magenta points). The volume was determined from Le Bail refinements of the corresponding XRD patterns.

## 3. Luminescence properties

The **LaMOF** compound was easily doped by small contents of the optically active ions $Eu^{3+}$ and $Tb^{3+}$. All doped materials, namely **LaMOF-1%Eu**, **LaMOF-1%Tb**, and **LaMOF-Eu-Tb** were isostructural to the **LaMOF** as confirmed by XRD, FTIR and thermal analyses (Figures S15-S17).

Solid-state luminescence behaviour of **LaMOF** was investigated as a potential blue emitter for the generation of white emission compound. Under UV irradiation ($\lambda_{exc}$ = 340 nm), **LaMOF** exhibits a broad emission band centred at 400 nm (Figure S18) corresponding to the $\pi$-$\pi^*$ transition of the ligand. Thus, **LaMOF** gets a blue emission with CIE chromatic coordinates equal to (0.1836, 0.1259) (Figure S19). Compared to the emission of the pure ligand (Figure S5 in reference 23)[28], a small red-shift is observed for the coordinated ligand, which may result from a slight change in intra- and inter-molecular interactions between ligands [15].

Doping LaMOF with 1% of $Tb^{3+}$ or $Eu^{3+}$ leads to the formation of crystals with a perfectly homogeneous luminescence (Figure S20). The emission spectra of doped compounds, **LaMOF-1%Eu** and **LaMOF-1%Tb**, are composed of the ligand-based blue emission and of the characteristic sharp lines of $Eu^{3+}$ and $Tb^{3+}$ ions corresponding to the $^5D_0 \rightarrow {}^7F_J$ (J = 0-4) $Eu^{3+}$ transitions and to the $^5D_4 \rightarrow {}^7F_J$ (J = 3-6) $Tb^{3+}$ transitions. Excitation spectra were monitored at different emission wavelengths, within the emission band of the ligand ($\lambda_{em}$ = 400 nm) within the $^5D_0 \rightarrow {}^7F_2$ $Eu^{3+}$ transition (615 nm) and within the $^5D_4 \rightarrow {}^7F_5$ $Tb^{3+}$ transition (545 nm) (Figures 3a and 4a). It then becomes clear that it is possible to modulate the emission of the ligand in relation to the emission of the lanthanide with the excitation wavelength. The excitation wavelength impacts the transferred energy form the ligand to the $Ln^{3+}$ cations to allow the coexistence of the

ligand and $Ln^{3+}$ ions emissions but also to modulate the emission intensities of the three colours[20]. Thus four different excitation wavelengths have been chosen: 258 and 289 nm where the $Ln^{3+}$ emission is more intense than the blue ligand emission, 321 nm where the ligand emission is significantly predominant and 312 nm where both emissions are more balanced. Emission spectra have been recorded for each excitation wavelength (Figures 3b and 4b) and CIE parameters were calculated each time. Thus, the CIE coordinates of **LaMOF-1%Eu** vary linearly from red to violet with an increase of the excitation wavelength while the CIE data of **LaMOF-1%Tb** move from green to cyan (Figures 3b and 4b). Emission lifetimes were determined for the $^5D_0 \rightarrow {}^7F_2$ $Eu^{3+}$ transition in **LaMOF-1%Eu**, and for the $^5D_4 \rightarrow {}^7F_5$ $Tb^{3+}$ transition in **LaMOF-1%Tb** (Table 1), where a monoexponential behaviour was observed for all compounds. The average lifetime for the $Eu^{3+}$ main emission is 600µs while it is equal to 1.23ms for the $Tb^{3+}$ main emission. Finally, the three doped samples exhibit a quite moderate quantum yield with an average value of 10%.

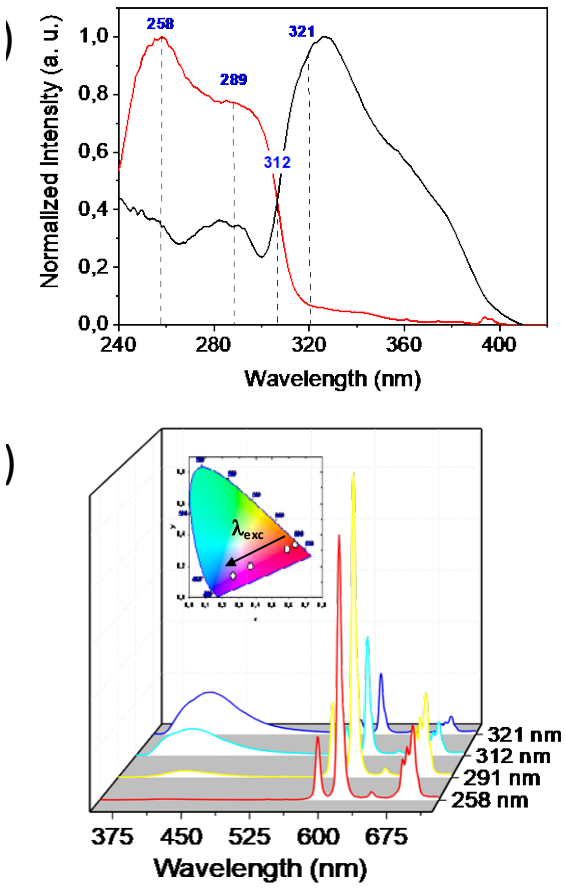


**Figure 3.** a) PLE spectra of **LaMOF-1%Eu** monitored at $\lambda_{em}$ = 425 nm (black line), within the ligand emission band, and monitored at $\lambda_{em}$ = 615 nm (red line), within the $^5D_0 \rightarrow {}^7F_2$ $Eu^{3+}$ transition. b) PL spectra of **LaMOF-1%Eu** monitored at different excitation wavelengths and corresponding CIE parameters reported on a chromaticity diagram.

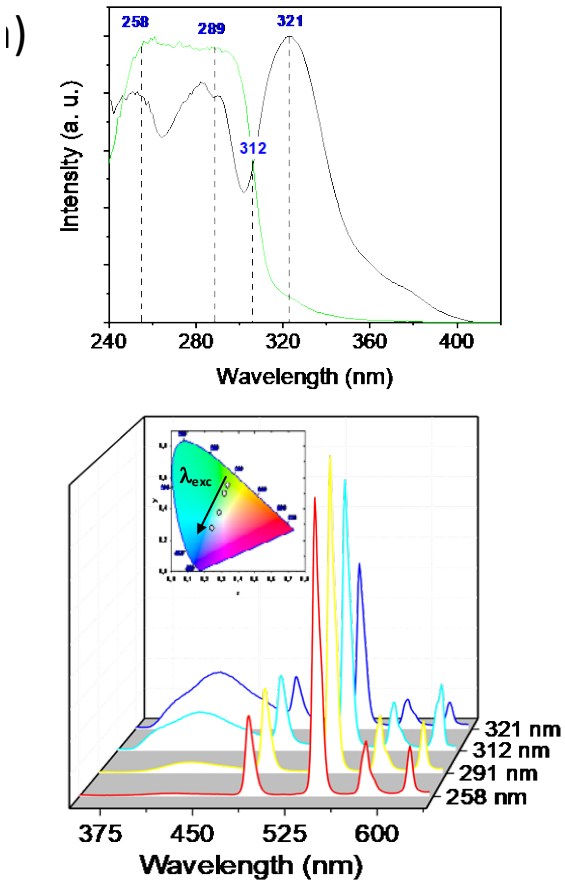


**Figure 4.** a) PLE spectra of **LaMOF-1%Tb** monitored at $\lambda_{em}$ = 425 nm (black line), within the ligand emission band, and monitored at $\lambda_{em}$ = 543 nm (green line), within the $^5D_4 \rightarrow {}^7F_5$ $Tb^{3+}$ transition. b) PL spectra of **LaMOF-1%Tb** monitored at different excitation wavelengths and corresponding CIE parameters reported on a chromaticity diagram.

The white-light emitting materials can be designed as a single phase by an adjustment of each colour emission intensities, which is possible by a fine control of $Eu^{3+}$ and $Tb^{3+}$ content but also by varying the excitation wavelength. The amount of $Eu^{3+}$ was deliberately chosen far less than that of $Tb^{3+}$ because the latter has a high efficiency due to the lowest emitting level $Eu^{3+}$ (17500 $cm^{-1}$) compared to the $Tb^{3+}$ (20500 $cm^{-1}$). Thus, after a careful screening, the compound **LaMOF-Eu-Tb** was obtained, with a molar content of $Tb^{3+}$ and $Eu^{3+}$ equal to 1%, and 0.25%, respectively.

Emission spectra have been monitored at the four different excitation wavelength and CIE parameters were calculated and reported on the chromaticity diagram (Figure 5). As expected, the corresponding luminescence emission of **LaMOF-Eu-Tb** falls in the white light region with CIE coordinates on the range of (0.3440, 0.3735) to (0.2679, 0.3014) when the excitation wavelength varies between 312 and 321 nm.

Emission lifetimes were also determined for the $^5D_0 \rightarrow {}^7F_2$ $Eu^{3+}$ transition and the $^5D_4 \rightarrow {}^7F_5$ $Tb^{3+}$ transition in **LaMOF-Eu-Tb** (Table 2). Then, the $Tb^{3+}$-to-$Eu^{3+}$ energy transfer rate and the transfer efficiency were determined from Equation (1) [37–39]:

$$\eta_{ET} = 1 - \frac{\tau}{\tau_0} \quad (1)$$

where $\tau$ and $\tau_0$ corresponding to the lifetimes of the donor in the presence and absence of the acceptor, respectively. Although the contents of $Eu^{3+}$ and $Tb^{3+}$ are low, there is little $Tb^{3+}$-to-$Eu^{3+}$ energy transfer which ranging from 1.51% to 10.71% when the excitation wavelength increases (Table 2). Consequently, the excitation wavelength influences the antenna effect of the ligand but also the $Tb^{3+}$-to-$Eu^{3+}$ energy transfer which is a crucial parameter to equilibrate the green-red balance.[40–42]

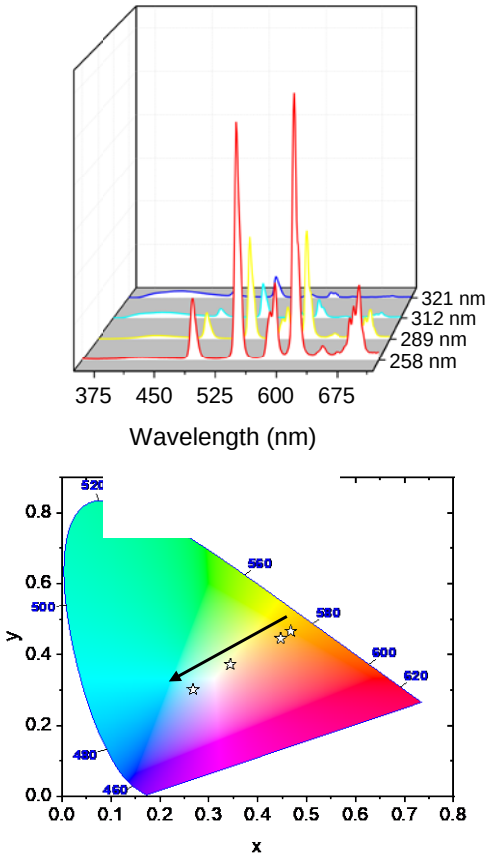


**Figure 5**. a) PL spectra of **LaMOF-Eu-Tb** monitored at different excitation wavelengths and b) corresponding CIE parameters reported on a chromaticity diagram.

**Table 2.** Decay times values for **LaMOF-1%Eu**, **LaMOF-1%Tb** and **LaMOF-Eu-Tb** compounds, and $Tb^{3+}$-to-$Eu^{3+}$ energy transfer efficiency in the bimetallic material.

| | **LaMOF-1%Eu** | **LaMOF-1%Tb** | **LaMOF-EuTb** | | |
|---|---|---|---|---|---|
| ***Excitation wavelength*** | $^5D_0 \rightarrow {}^7F_2$ $Eu^{3+}$ | $^5D_0 \rightarrow {}^7F_2$ $Tb^{3+}$ | $^5D_0 \rightarrow {}^7F_2$ $Eu^{3+}$ | $^5D_0 \rightarrow {}^7F_2$ $Tb^{3+}$ | ET efficiency (%) |
| 258 nm | 594 ± 2 µs | 1.26 ± 0.01 ms | 594 ± 4 µs | 1.241 ± 0.006 ms | 1.51 |
| 289 nm | 569 ± 4 µs | 1.269 ± 0.007 ms | 598 ± 4 µs | 1.216 ± 0.009 ms | 3.49 |
| 312 nm | 580 ± 5 µs | 1.207 ± 0.008 ms | 630 ± 12 µs | 1.17 ± 0.01 ms | 7.14 |
| 321 nm | 649 ± 4µs | 1.176 ± 0.004 ms | 715 ± 7 µs | 1.125 ± 0.02 ms | 10.71 |

## CONCLUSION

Two new lanthanide MOF built upon isophthalate, $Ln_{1.14}Na_{0.57}(BDC)_2(H_2O)\cdot 4H_2O$ (Ln = $La^{3+}$ or $Ce^{3+}$), were synthesized by the hydrothermal conversion of a coordination compound. The three-dimensional network consists in chains of face-sharing $[LnO_{10}]$ polyhedra connected by the linker molecules to form alternating polar and apolar channels. The latter are occupied by water molecules and disordered $Ln^{3+}$ and $Na^{+}$ cations provided from the basic solution used during the synthesis. The dehydration process was investigated by thermodiffraction. When the water molecules are removed, one observes a shrink of the lattice volume leading to a non porous character. This process was found to be irreversible both in air and in suspension of various solvents, in line with the strong structural reorganization occurring around the $Ln^{3+}$ cations. Finally, the **LaMOF** counterpart has been easily doped by $Eu^{3+}$ and $Tb^{3+}$ in appropriate ratios to provide a white emission material. The tuning of the excitation wavelength enables the modulation of the antenna effect from the ligand to the $Ln^{3+}$ emitting levels but also the variation of the $Tb^{3+}$-to-$Eu^{3+}$ energy transfer efficiency. Consequently, a fine adjustment of the excitation wavelength allowed to get emission in the white domain (CIE coordinates (0.3440, 0.3735) at $\lambda_{exc}$ = 312 nm).

## EXPERIMENTAL SECTION

**Chemicals and Materials**. $CeCl_3\cdot 7H_2O$ (Aldrich, 99.9%), $La(NO_3)_3\cdot 6H_2O$ (Alfa Aesar, 99.9%), $TbCl_3\cdot 6H_2O$ (Alfa Aesar, 99.99%), $Eu(NO_3)_3\cdot 6H_2O$ (Alfa Aesar, 99.99%) and 1,3-$H_2$BDC (Alfa Aesar, 98%) were used without further purification.

**Synthesis of CeMOF.** 1,3-$H_2$BDC (574 mg, 3.46 mmol) was dissolved in 11 mL of an aqueous NaOH solution (0.70 M) while $CeCl_3 \cdot 7H_2O$ (645 mg, 1.73 mmol) was dissolved in 2 mL dezionized water. The two solutions were mixed under stirring and a white precipitate was formed (**Ce-CP**). The pH of the mixture was adjusted at 5 by addition of small amount of an HCl solution (1 M) to obtain the formation of a white precipitate. Then, the above mixture was placed in a sealed 21 ml Teflon-lined stainless vessel, which was heated at 150°C for 3 days under autogenous pressure and cooled down to room temperature. Colorless needle-like crystals were obtained. Yield: 80.3%. Anal. Calcd for $Ce_{1.14}Na_{0.57}C_{16}O_{13}H_{18}$ (%): C, 32.51; H, 3.05. Found: C, 32.03; H, 2.93. IR (KBr pellet, $cm^{-1}$): 1676 (sh),1616 (vs), 1599 (vs), 1541 (vs), 1511 (s), 1475 (s), 1452 (vs), 1389 (vs), 1313 (m), 1275 (m), 1155 (m), 1072 (m), 926 (m), 820 (m), 743 (s), 710 (s), 658 (m), 569 (m), 521 (m) and 422 (m).

**Synthesis of LaMOF.** 1,3-$H_2$BDC (574 mg, 3.46 mmol) was dissolved in 11 mL of an aqueous NaOH solution (0.70 M) while $La(NO_3)_3 \cdot 6H_2O$ (750 mg, 1.73 mmol) was dissolved in 2 mL dezionized water. The two solutions were mixed under stirring and a white precipitate was formed (**La-CP**). The pH of the mixture was adjusted at 5 by addition of small amount of an HCl solution (1 M) to obtain the formation of a white precipitate. Then, the above mixture was placed in a sealed 21 ml Teflon-lined stainless vessel, which was heated at 180°C for 5 days under autogenous pressure and cooled down to room temperature. Colorless needle-like crystals were obtained. Yield: 85.9%. Anal. Calcd for $La_{1.14}Na_{0.57}C_{16}O_{13}H_{18}$ (%): C, 32.80; H, 3.07. Found: C, 32.70; H, 3.02. IR (KBr pellet, $cm^{-1}$): 1668 (sh),1612 (vs), 1599 (vs), 1541 (vs), 1510 (s), 1475 (s), 1452 (vs), 1389 (vs), 1315 (m), 1275 (m), 1155 (m), 1072 (m), 924 (m), 820 (m), 743 (s), 710 (s), 658 (m), 569 (m), 519 (m) and 422 (m).

**Synthesis of LaMOF-1%Eu.** The procedure was the same as that for **LaMOF** except that the cationic solution was composed by $La(NO_3)_3 \cdot 6H_2O$ (742 mg, 1.71 mmol) and $Eu(NO_3)_3 \cdot 6H_2O$ (7.4 mg, 0.02 mmol). Yield: 82.3%. The Eu/La ratio was determined by ICP-AES to be equal to 1.08%.

**Synthesis of LaMOF-1%Tb.** The procedure was the same as that for **LaMOF** except that the cationic solution was composed by $La(NO_3)_3 \cdot 6H_2O$ (742 mg, 1.71 mmol) and $TbCl_3 \cdot 6H_2O$ (6.5 mg, 0.02 mmol). Yield: 78.8%. The Tb/La ratio was determined by ICP-AES to be equal to 1.02%.

**Synthesis of LaMOF-Eu-Tb.** The procedure was the same as that for **LaMOF** except that the cationic solution was composed by $La(NO_3)_3 \cdot 6H_2O$ (741 mg, 1.71 mmol), $Eu(NO_3)_3 \cdot 6H_2O$ (1.9 mg, 0.004 mmol), and $TbCl_3 \cdot 6H_2O$ (6.5 mg, 0.02 mmol). Yield: 81.9%. The Eu/La and Tb/La ratio were determined by ICP-AES to be equal to 0.21% and 1.03%, respectively.

**Characterization**

Powder X-ray Diffraction spectra were monitored using a D8 Bruker diffractometer in the Bragg-Brentano geometry, equipped with a front germanium monochromator, a copper anode (CuK-L3 radiation λ=1.540598 Å) and a LynxEye PSD detector. Le Bail refinements were performed with the full-matrix least-squares technique using the Jana2006 program[43]. The errors bars on all parameters were calculated as three times the Berar's[44] coefficient multiplied by the standard deviation. FTIR spectra were recorded in the 4000-400 $cm^{-1}$ range on a Bruker Vertex equipped with a computer control using the OPUS software. Thermogravimetric analysis (TGA) was performed by flowing dry air with a heating and cooling rate of 5°C/min on a SETARAM TG-DSC 111 between 20 and 800°C. Room-temperature photoluminescence spectra were recorded on a Jobin-Yvon Fluorolog 3 fluorimeter equipped with a CCD camera (excitation

source: 450 W Xe arc lamp). The emission spectra were corrected for detection and optical spectral response of the spectrofluorimeter and the excitation spectra were weighed for the spectral distribution of the lamp intensity using a photodiode reference detector. Quantum yields have been performed with a integration sphere connected to our device.

Single crystals were selected and isolated using an optical microscope; they were mounted on MicroMount needles (MiTeGen). X-ray single crystal data were collected on an APEX II Quazar diffractometer (4-circle Kappa goniometer, IμS microfocus source (Mo Kα), CCD detector). The structures were determined by direct methods with SHELXS-97 and SHELXL-97 programs included in WINGX package[45,46]. All non–hydrogen atoms positions were refined anisotropically. Hydrogen atoms of the carboxylate molecules were geometrically constrained (HFIX options) whereas hydrogen atoms of the coordinated water molecules were constrained with DFIX options. The hydrogen atoms of free water molecules were not placed. The assignment of the atoms in metal/alkaline environments was based on M-O distances and thermal motion considerations (Table S1-S6).[47–49] The conditions of data collection are summarized in Table 1.[50]

Crystallographic data (excluding structure factors) for structures have been deposited with the Cambridge Crystallographic Data Centre as supplementary publication nos. 2013537 ($Ce_{1.14}Na_{0.57}C_{16}O_9H_{18}$) and 2013538 ($La_{1.14}Na_{0.57}C_{16}O_9H_{18}$). Copies of the data can be obtained, free of charge, on application to CCDC, 12 Union Road, Cambridge CB2 1EZ, UK, (fax: +44 1223 336033 or e-mail: deposit@ccdc.cam.ac.uk).

Keywords : metal-organic frameworks, lanthanide, thermal behaviour, white luminescence

ACKNOWLEDGMENT

The authors attached to the IMMM institute gratefully acknowledge the "X-ray Diffusion and Diffraction" technical platform of IMMM (Le Mans University). V.T. thanks la Fondation de la Maison de la Chimie for his postdoctoral fellowship.

REFERENCES


[1] W. P. Lustig, S. Mukherjee, N. D. Rudd, A. V. Desai, J. Li, S. K. Ghosh, *Chem. Soc. Rev.* **2017**, *46*, 3242–3285.

[2] F. Artizzu, F. Quochi, A. Serpe, *Inorg. Chem. Front.* **2015**, *2*, 213–222.

[3] J. Rocha, C. D. S. Brites, L. D. Carlos, *Chem. – A Eur. J.* **2016**, *22*, 14782–14795.

[4] Z. Hu, B. J. Deibert, J. Li, *Chem Soc Rev* **2014**, *43*, 5815–5840.

[5] N. Busschaert, C. Caltagirone, W. Van Rossom, P. A. Gale, *Chem. Rev.* **2015**, *115*, 8038–8155.

[6] Y. Cui, F. Zhu, B. Chen, G. Qian, *Chem. Commun.* **2015**, *51*, 7420–7431.

[7] D. Tian, Y. Li, R. Y. Chen, Z. Chang, G. Y. Wang, X. H. Bu, *J. Mater. Chem. A* **2014**, *2*, 1465–1470.

[8] X. L. Zhao, D. Tian, Q. Gao, H. W. Sun, J. Xu, X. H. Bu, *Dalt. Trans.* **2016**, *45*, 1040–1046.

[9] L. Xu, Y. Li, Q.-J. Pan, D. Wang, S. Li, G. Wang, Y. Chen, P. Zhu, W. Qin, *ACS Appl. Mater. Interfaces* **2020**, *12*, 18934–18943.

[10] W. P. Lustig, Z. Shen, S. J. Teat, N. Javed, E. Velasco, D. M. O'Carroll, J. Li, *Chem. Sci.* **2020**, *11*, 1814–1824.

[11] F. Igoa, G. Peinado, L. Suescun, C. Kremer, J. Torres, *J. Solid State Chem.* **2019**, *279*,

120925.

[12] N. Zhang, Q. Guan, C. Liu, Y. Sun, B. Li, Y. Xing, F. Bai, *Appl. Organomet. Chem.* **2020**, *34*, DOI 10.1002/aoc.5506.

[13] H. S. Jena, A. M. Kaczmarek, C. Krishnaraj, X. Feng, K. Vijayvergia, H. Yildirim, S. N. Zhao, R. Van Deun, P. Van Der Voort, *Cryst. Growth Des.* **2019**, *19*, 6339–6350.

[14] J. Wu, H. Zhang, S. Du, *J. Mater. Chem. C* **2016**, *4*, 3364–3374.

[15] Y. W. Zhao, F. Q. Zhang, X. M. Zhang, *ACS Appl. Mater. Interfaces* **2016**, *8*, 24123–24130.

[16] Y. Gai, Q. Guo, K. Xiong, F. Jiang, C. Li, X. Li, Y. Chen, C. Zhu, Q. Huang, R. Yao, M. Hong, *Cryst. Growth Des.* **2017**, *17*, 940–944.

[17] Y. Y. An, L. P. Lu, S. S. Feng, M. L. Zhu, *CrystEngComm* **2018**, *20*, 2043–2052.

[18] L. Qiu, C. Yu, X. Wang, Y. Xie, A. M. Kirillov, W. Huang, J. Li, P. Gao, T. Wu, X. Gu, Q. Nie, D. Wu, *Inorg. Chem.* **2019**, *58*, 4524–4533.

[19] Q. Li, J. Qian, J. Zhou, L. Du, Q. Zhao, *CrystEngComm* **2020**, *22*, 2667–2674.

[20] J. J. Huang, J. H. Yu, F. Q. Bai, J. Q. Xu, *Cryst. Growth Des.* **2018**, *18*, 5353–5364.

[21] M. Yu, X. Yao, X. Wang, Y. Li, G. Li, *Polymers (Basel).* **2019**, *11*, 99.

[22] H. Yan, H. Ni, J. Jia, C. Shan, T. Zhang, Y. Gong, X. Li, J. Cao, W. Wu, W. Liu, Y. Tang, *Anal. Chem.* **2019**, *91*, 5225–5234.

[23] N. Zhang, Q. Guan, C. Liu, Y. Sun, B. Li, Y. Xing, F. Bai, *Appl. Organomet. Chem.* **2020**,

*34*, DOI 10.1002/aoc.5506.

[24] M. L. Ma, C. Ji, S. Q. Zang, *Dalt. Trans.* **2013**, *42*, 10579–10586.

[25] Y. Yang, L. Chen, F. Jiang, M. Yu, X. Wan, B. Zhang, M. Hong, *J. Mater. Chem. C* **2017**, DOI 10.1039/C6TC05316E.

[26] D. F. He, F. jiang Zhou, J. J. Deng, F. Luo, H. Xue, F. kun Meng, L. qun Sun, H. sheng Liu, S. X. Liu, *Inorg. Chem. Commun.* **2018**, *96*, 43–46.

[27] P. Mahata, K. V Ramya, S. Natarajan, *Dalt. Trans.* **2007**, 4017–4026.

[28] I. N'Dala-Louika, D. Ananias, C. Latouche, R. Dessapt, L. D. Carlos, H. Serier-Brault, *J. Mater. Chem. C* **2017**, *5*, 10933–10937.

[29] F. Zarekarizi, A. Morsali, *Inorg. Chem.* **2020**, *59*, 2988–2996.

[30] Y. Ge, B. Teng, L. Lv, R. Chen, B. Wu, *Cryst. Growth Des.* **2020**, *20*, 486–497.

[31] Y. Pan, W. Liu, D. Liu, Q. Ding, J. Liu, H. Xu, M. Trivedi, A. Kumar, *Inorg. Chem. Commun.* **2019**, *100*, 92–96.

[32] S. Kuno, H. Akeno, H. Ohtani, H. Yuasa, *Phys. Chem. Chem. Phys.* **2015**, *17*, 15989–15995.

[33] Y. Zheng, K. Liu, H. Qiao, Y. Zhang, Y. Song, M. Yang, Y. Huang, N. Guo, Y. Jia, H. You, *CrystEngComm* **2011**, *13*, 1786.

[34] C. C. R. Sutton, G. da Silva, G. V. Franks, *Chem. - A Eur. J.* **2015**, *21*, 6801–6805.

[35] Q.-D. Liu, J.-R. Li, S. Gao, B.-Q. Ma, F.-H. Liao, Q.-Z. Zhou, K.-B. Yu, *Inorg. Chem.*

*Commun.* **2001**, *4*, 301–304.

[36] T. Devic, V. Wagner, N. Guillou, A. Vimont, M. Haouas, M. Pascolini, C. Serre, J. Marrot, M. Daturi, F. Taulelle, G. Férey, *Microporous Mesoporous Mater.* **2011**, *140*, 25–33.

[37] L. J. Charbonniere, N. Hildebrandt, R. F. Ziessel, H.-G. Loehmannsroeben, *J. Am. Chem. Soc.* **2006**, *128*, 12800–12809.

[38] H.-Y. D. Ke, E. R. Birnbaum, *J. Lumin.* **1995**, *63*, 9–17.

[39] A. N. Carneiro Neto, R. T. Moura, A. Shyichuk, V. Paterlini, F. Piccinelli, M. Bettinelli, O. L. Malta, *J. Phys. Chem. C* **2020**, *10*, DOI 10.1021/acs.jpcc.0c00759.

[40] J. Yang, X. Wang, L. Song, N. Luo, J. Dong, S. Gan, L. Zou, *Opt. Mater. (Amst).* **2018**, *85*, 71–78.

[41] Y. Zhang, J. Zhang, X. Li, X. Jiang, J. Shi, Y. Wen, *J. Mater. Sci. Mater. Electron.* **2018**, *29*, 3120–3126.

[42] T. Li, P. Li, Z. Wang, S. Xu, Q. Bai, Z. Yang, *Dalt. Trans.* **2015**, *44*, 16840–16846.

[43] V. Petricek, M. Dusek, L. Palatinus, **2006**.

[44] J. F. Bérar, P. Lelann, *J. Appl. Crystallogr.* **1991**, *24*, 1–5.

[45] M. Sheldrick, G., Göttingen University, **1986**.

[46] M. Sheldrick, G., Göttingen University, **1997**.

[47] I. D. Brown, D. Altermatt, *Acta Crystallogr. Sect. B* **1985**, *41*, 244–247.

[48] N. E. Brese, M. O'Keeffe, *Acta Crystallogr. Sect. B* **1991**, *47*, 192–197.

[49] W. Liu, H. H. Thorp, *Inorg. Chem.* **1993**, *32*, 4102–4105.

[50] L. Spek, A., Utrecht University, **2002**.